Journal of Alloys and Compounds 362 (2004) 83–87

Journal of ALLOYS AND COMPOUNDS

www.elsevier.com/locate/jallcom

Application of SRIXE and XANES to the determination of the oxidation state of iron in prostate tissue sections

W.M. Kwiatek [a,*], A.L. Hanson [b], C. Paluszkiewicz [c,d], M. Gałka [e], M. Gajda [f], T. Cichocki [f]

[a] *Henryk Niewodniczański Institute of Nuclear Physics, ul. Radzikowskiego 152, PL-31-342 Cracow, Poland*
[b] *Brookhaven National Laboratory, DAT, Upton, NY 11973, USA*
[c] *Regional Laboratory, Jagiellonian University, ul. Karasia 3, PL-30-059 Cracow, Poland*
[d] *University of Mining and Metallurgy, al. Mickiewicza 30, PL-30-059 Cracow, Poland*
[e] *Gabriel Narutowicz Hospital, ul. Prądnicka 37, PL-31-202 Cracow, Poland*
[f] *Collegium Medicum, Jagiellonian University, ul. Kopernika 7, PL-31-034 Cracow, Poland*

Received 15 February 2003; received in revised form 16 April 2003; accepted 21 April 2003

Abstract

Normal prostate and cancerous prostate tissue sections were analyzed using synchrotron radiation-induced X-ray emission and X-ray absorption near-edge structure (XANES) at the X-26A microprobe beam line located at the National Synchrotron Light Source, Brookhaven National Laboratory, USA. In both measurements, a monochromatic beam of size of 16×14 μm^2 was applied. Two-dimensional scans of selected areas of non-cancerous and cancerous tissue sections were performed in order to obtain the distributions of various trace element concentrations. The XANES spectra were recorded for selected points containing high concentrations of iron. These measurements were performed with the aim of determining the oxidation state of iron. It was found that the iron concentration was much higher in the cancerous sections of the analyzed tissues than in the non-cancerous sections. From the results of XANES spectra analysis, iron in cancerous prostate tissue sections mostly occurs in the $+3$ oxidation state.

Keywords: Synchrotron radiation; XANES; Pre-peak; Prostate; Trace elements; Oxidation state

1. Introduction

The aim of this study was to determine the concentration and oxidation states of transition metals in biological tissues. The increase in concentration of some trace elements in prostate cancer (prostate carcinoma) has prompted the investigation of the genesis of this phenomenon. Prostate cancer is the most common disease among men. The understanding of its genesis is incomplete and therefore this kind of investigation is being performed. Trace elements play a significant role in biological tissues, but some are carcinogenic to humans [1]. Some elements, such as Ti, V, Cr, Mn, Pb and Cd, are recognized as toxic and carcinogenic, while the carcinogenicity of others has not been determined. Some elements which present elevated concentrations in cancerous tissues may be toxic [2]. The increased concentration of iron in tissue sections is due to its catalytic role in the Fenton reaction [2,3]. It is known that cancerous cells require oxygen for growth. The Fenton reaction may explain the production of the free radicals responsible for cancer growth. The Fenton reaction consists of two co-operative stages [3]:

$$Fe^{2+} + H_2O_2 \rightarrow^{*} OH + OH^{-} + Fe^{3+}$$

$$O_2^{*-} + Fe^{3+} \rightarrow O_2 + Fe^{2+}$$

Thus, determination of the presence of Fe^{2+} and Fe^{3+} may help elucidate the mechanism of damage of genetic material in cells by the chemically active oxygen-containing molecules called free radicals.

2. Material

Samples for this study were obtained as a result of the surgical treatment of prostate cancer disease. The surgery—*radical prostatectomy*—was performed at the Gabriel Naru-

* Corresponding author. Tel.: +48-12-662-8235; fax: +48-12-662-8428.
E-mail address: wojciech.kwiatek@ifj.edu.pl (W.M. Kwiatek).

0925-8388/$ – see front matter © 2003 Elsevier B.V. All rights reserved.
doi:10.1016/S0925-8388(03)00566-8

Table 1
Elemental content of MULTI-I and MULTI-II standards

Element	Chemical formula	MULTI-I (μg/g)	MULTI-II (μg/g)
K	KNO_3	NA	7.593 ± 0.368
Ca	$Ca(NO_3)_2$	8.923 ± 0.152	NA
V	V_2O_3	9.901 ± 0.108	9.901 ± 0.108
Mn	$Mn(NO_3)_2$	NA	10.386 ± 0.191
Fe	$Fe(NO_3)_2$	10.380 ± 0.076	10.848 ± 0.182
Zn	$Zn(NO_3)_2$	10.738 ± 0.061	11.352 ± 0.140
As	$As(NO_3)_2$	6.861 ± 0.079	NA
Hg	$Hg(NO_3)_2$	NA	9.784 ± 0.262
Pb	$Pb(NO_3)_2$	11.460 ± 0.114	NA
Sr	$Sr(NO_3)_2$	11.491 ± 0.068	11.657 ± 0.151
Zr	$ZrCl_4$	15.119 ± 0.248	17.061 ± 0.563
Mo	$(NH_4)_2MoO_4$	2.129 ± 0.058	2.755 ± 0.141
Cd	$Cd(NO_3)_2$	7.070 ± 0.734	NA

NA, not applied.

towicz Hospital (Cracow, Poland). The average age of the patients was 61 years. There were three patients diagnosed with *Adenocarcinoma prostate*.

After the tumor had been removed it was investigated by histopathologists. Selected parts of cancerous and non-cancerous tissues were frozen in liquid nitrogen for 1 h. The samples were then cut on a cryomicrotome into 12 μm thick sections. These sections were placed on 3 μm thick Mylar foil. Adjacent sections were placed on a microscopic glass slide for staining and further histological study. The stained section was used for cancer classification and for selection of the area to be analyzed by SRIXE and XANES.

For trace element determination and quality control of the SRIXE method, two 10 μm thick multielemental standards were prepared [4]. Pure acrylamide, *N*,*N*′-methylenebisacrylamide, was mixed with different aqueous solutions of metal nitrates. In standard MULTI-I the solutions include metals such as Ca, V, Fe, Zn, As, Pb, Sr, Zr, Mo, and Cd, and in standard MULTI-II the solutions include metals such as K, V, Mn, Fe, Zn, Hg, Pb, Sr, Zr, and Mo. Although the metal concentration was calculated to be 10 μg/g final solution, the measured concentrations determined with total reflection X-ray fluorescence gave slightly different results (see Table 1). These values were taken into account when calculating the elemental concentrations.

3. Methods

The SRIXE method has already been described [5,6]. Measurements were performed at the X26A beam line at the National Synchrotron Light Source, Brookhaven National Laboratory, USA. The beam line is equipped with standard apparatus for SRIXE measurements as described by Hanson et al. [7] and the selection of experimental conditions is described by Kwiatek et al. [8]. Additionally, the beam line is equipped with an ellipsoidal mirror that can focus monochromatic X-rays with an 8:1 ratio [9]. The use of this platinum-coated mirror reduces all third- and higher-order harmonic X-rays transmitted through the channel cut Si ⟨111⟩ monochromator placed in the beam path between the primary aperture and the mirror. The spectra were recorded with a conventional Si(Li) detector with an energy resolution of 140 eV at 5.9 keV X-ray energy. The SRIXE measurements were performed with a monochromatic beam of 17 and 7.2 keV. The spectra for single point analysis were usually collected for 300 s live time, while two-dimensional mapping was acquired for 2 s/pixel with a 15 μm step in the *X* and *Y* directions. Typical scan areas were 300×300 and 500×500 μm^2.

The XANES measurements were performed at the same beam line using the experimental apparatus described by Sutton et al. [10]. For this study the incident monochromatic energy was scanned in about 0.3 eV steps over the range from approximately −20 to +50 eV relative to the nominal absorption-edge energy for elemental iron (7.112 keV). The measurements were performed in fluorescence mode. The iron absorption edge was scanned with a lifetime of 10 s/monochromator step. For both SRIXE and XANES measurements the beam size was set to 16×14 μm^2. The XANES measurements were performed in selected areas of the samples which were recognized as rich in iron content. These areas were determined by means of two-dimensional SRIXE scanning.

4. Results and discussion

Several SRIXE point analyses were performed on each tissue section in order to determine the trace element concentrations. Fig. 1 shows two typical normalized X-ray fluorescence spectra for non-cancerous and cancerous prostate tissue sections. As can be seen there is no difference in the major elemental content, but there are differences in the trace element concentrations. Table 2 presents the average concentrations of the elements detected in the samples. Chlorine and potassium concentrations were not determined since these elements were used as tissue structure tracers due to their high abundance in tissues.

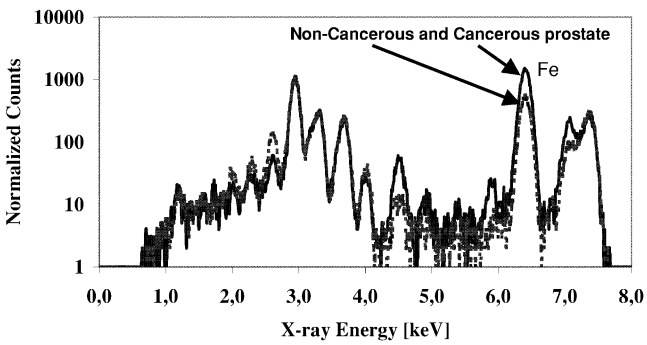

Fig. 1. Typical normalized X-ray fluorescence spectra for (a) non-cancerous and (b) cancerous prostate tissue sections.

Table 2
Average concentrations of trace elements in prostate tissue sections (μg/g dry weight)

Element	Non-cancerous sections	Cancerous sections
Ca	1870 ± 230	2240 ± 280
Ti	150 ± 35	ND
V	ND	20 ± 4
Cr	2.0 ± 0.5	7 ± 1
Mn	6.0 ± 1.1	8 ± 2
Fe	490 ± 60	1370 ± 70
Zn	110 ± 30	16.7 ± 3.5
Se	ND	11.5 ± 3.5

ND, not detected.

Fig. 2a and b show stained histological views of prostate tissues. The left view corresponds to non-cancerous (normal) prostate tissue, while the right view corresponds to the cancerous part of the tissue. The viewed areas were scanned with a micro-beam in order to determine the distributions of the trace elements within the tissue structure. Figs. 3a,b and 4a,b show two-dimensional scans of the tissue sections presented in Fig. 2 highlighting specific trace elements.

As can be seen, the chlorine distribution (similar results were obtained for potassium) corresponds to tissue structures, while that of iron does not. Iron is not uniformly distributed. White corresponds to the highest concentration of the element. For a better view of the iron concentration, the concentration scale in Fig. 4a has been expanded.

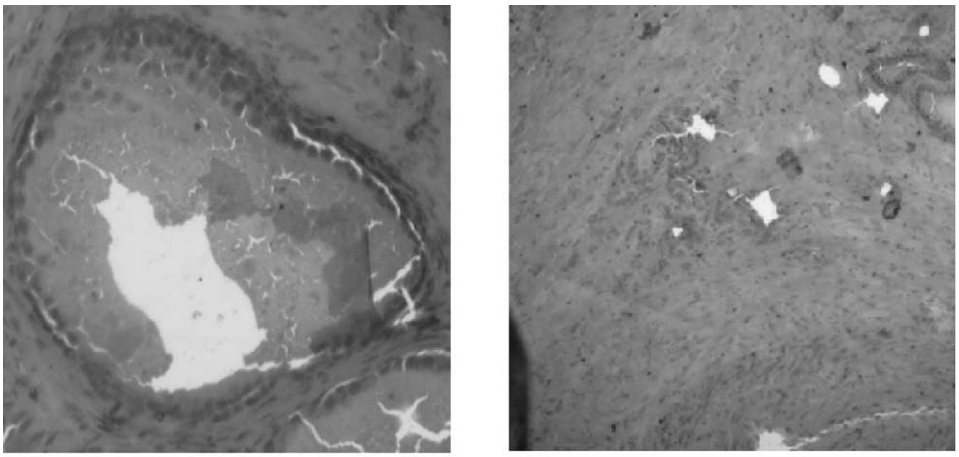

Fig. 2. (a) Non-cancerous (normal) prostate tissue section, (b) cancerous tissue section.

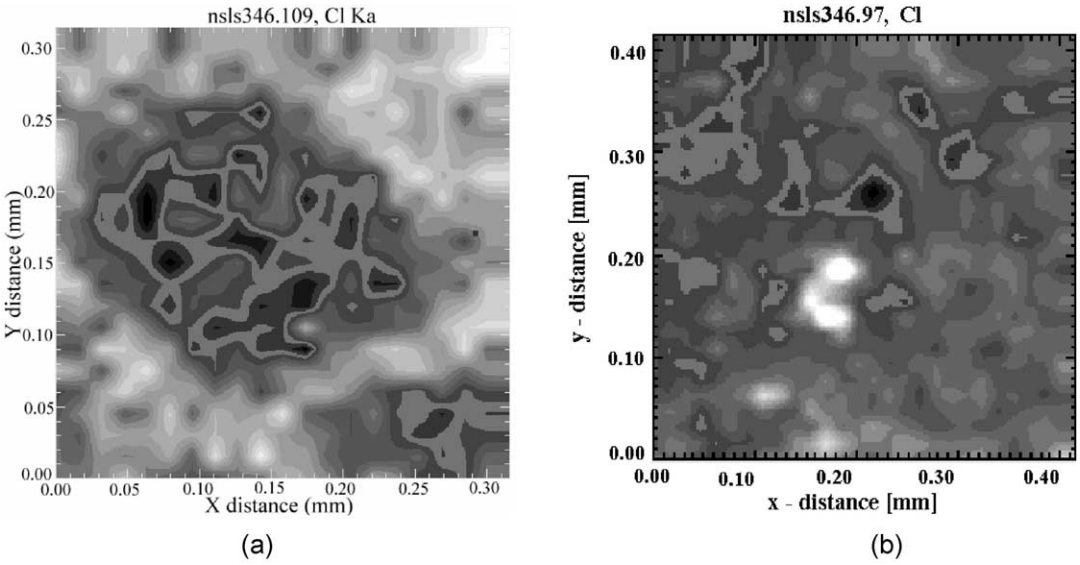

Fig. 3. Chlorine distribution in prostate tissue sections: (a) non-cancerous (normal) and (b) cancerous tissue.

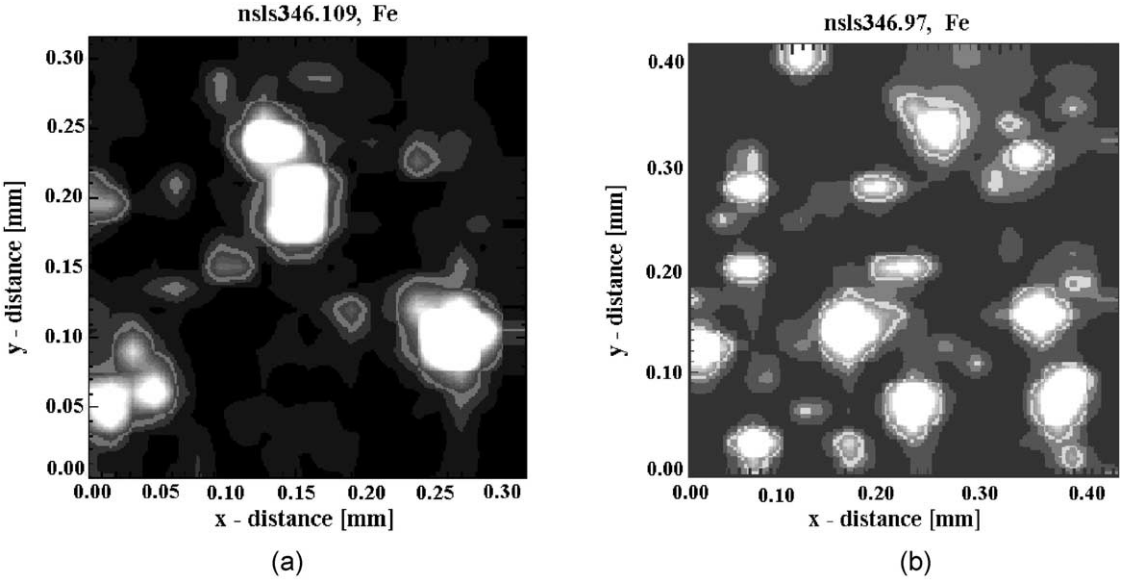

Fig. 4. Iron distribution in prostate tissue sections: (a) non-cancerous (normal) and (b) cancerous tissue.

Special attention was given to iron. In the two-dimensional map for iron, spots with high iron concentration can readily be observed. The XANES measurements were performed on these spots to determine the oxidation state of the iron.

For normalization and oxidation state determination, selected standards were measured. Following the work of Bajt et al. [11,12], we chose Synthetic Fayalite (Fe_2SiO_4: standard for Fe(II)), pure Magnetite ($FeO{\cdot}Fe_2O_3$: standard for a mixture of Fe(II) and Fe(III) in a ratio of 1:2) and pure Hematite (Fe_2O_3: standard for Fe(III)) as standards for the iron pre-edge peak position. The position of the pre-edge peak is linearly dependent on the energy of the emitted X-rays and depends on the oxidation state of iron. Therefore, it can be used to determine the oxidation state of the iron analyzed in the measured area. This was confirmed in our previous work while analyzing kidney tissues [13]. Also, the position of the iron absorption edge depends on the oxidation state. The position moves towards higher energies with a higher oxidation state of the element. The only difference was observed in the XANES spectra for pure Magnetite (Fe(II) + 2Fe(III)), where the pre-edge peak position was closer to the position of the pre-edge peak for Hematite (Fe(III)), while the absorption edge for Magnetite was closer to the position of the absorption edge for Fayalite (Fe(II)), which is shown in Fig. 5. This does not cause any problems in iron state determinations. Fig. 6 shows typical XANES spectra recorded at selected points of (a) a non-cancerous (normal) and (b) a cancerous prostate tissue section. According to the calibration of the iron pre-edge peak position [13] the well-defined pre-edge peak in the spectra shown in Fig. 6 indicates that iron occurs in the +3 oxidation state in the cancerous part of the prostate tissue, while in the

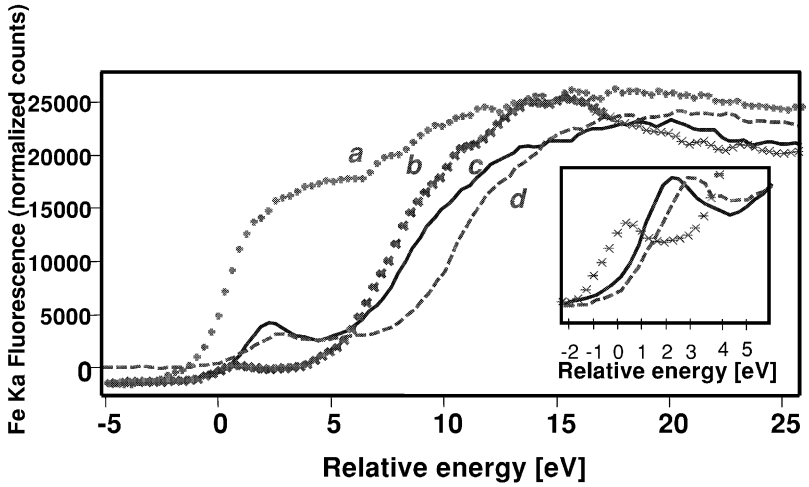

Fig. 5. XANES spectra for (a) pure iron foil, (b) Synthetic Fayalite, (c) Magnetite and (d) Hematite.

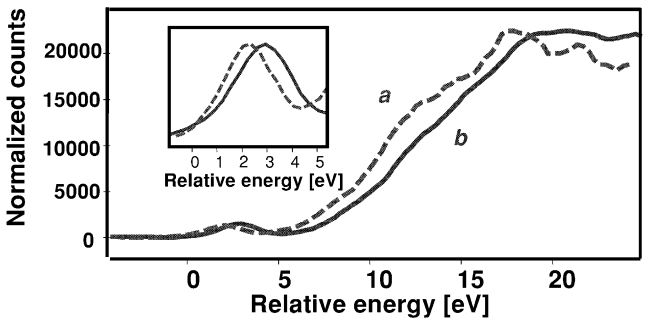

Fig. 6. Typical XANES spectra recorded for selected points of (a) a non-cancerous (normal) and (b) a cancerous prostate tissue section.

non-cancerous part the position of the pre-edge peak as well as the edge is shifted to lower energies, which indicates that iron occurs there at an oxidation state lower than +3.

5. Conclusions/summary

As shown in Table 2, the iron concentration was higher by a factor of 3 in cancerous parts of the analyzed tissue than in non-cancerous parts. At some locations, for a single analysis, the discrepancy in iron concentration reaches a factor of 10.

The results obtained from XANES show a difference in the oxidation state of iron between cancerous and non-cancerous parts of prostate tissue.

As a result of the Fenton reaction, an increase in the concentration of the hydroxyl radical (*OH) is observed. This radical is an active oxidizing agent and is able to induce the mutation of DNA in vivo [14,15]. The rate of the Fenton reaction depends on the availability of iron ions. The availability of iron is required for the division of normal and cancerous cells. Tumor growth depends on the iron concentration and is faster in an iron-rich environment [16].

The cancerous parts of prostate tissue are rich in iron, occurring mostly in the +3 oxidation state, and this demonstrates the presence of the Fenton reaction and the production of free radicals in cancerous tissues. SRIXE and XANES are two powerful, complementary techniques for studying the nature of cancer tissue. The results obtained provide additional information about cancer.

Acknowledgements

The authors wish to thank Dr. Thomas Brandenburg and Prof. Arnd Knöchel, Hamburg University, Germany, for their help with the multielemental standards preparation and TRXRF measurements. Special thanks to Prof. Jerzy Stachura and co-workers for their help with sample classification and cancer cell definition. Also, many thanks to Grace Shea-McCarty and Antonio Lanzirotti for their help during the experiments at beam line X26A. This work was supported by the State Committee for Scientific Research (KBN), Poland (grant No. IFJ0202), and the National Synchrotron Light Source (General User Grant No. 3680).

References

[1] P. Boffetta, Scand. J. Work Environ. Health 19 (Suppl. 1) (1993) 67–70.
[2] E.J. Lesnefsky, Adv. Exp. Med. Biol. 366 (1994) 129–146.
[3] B. Halliwell, J.M.C. Gutteridge, Biochem. J. 219 (1984) 1–14.
[4] Th. Brandenburg, Masters thesis, Hamburg University, 1992.
[5] K.W. Jones, in: R.E. Van Griken, A. Markowicz (Eds.), Synchrotron Radiation-induced X-ray Emission, Handbook of X-ray Spectrometry, Marcel Dekker, New York, 1992.
[6] W.M. Kwiatek, Acta Phys. Polon. A 86 (1994) 695–703.
[7] A.L. Hanson, K.W. Jones, B.M. Gordon, J.G. Pounds, W.M. Kwiatek, G.L. Long, M.L. Rivers, S.R. Sutton, Nucl. Instr. Meth. B 24/25 (1987) 400–404.
[8] W.M. Kwiatek, A.L. Hanson, K.W. Jones, Nucl. Instr. Meth. B 50 (1990) 347–352.
[9] K.W. Jones, P.Z. Takacs, J.B. Hastings, J.M. Casstevens, C.D. Pionke, Proc. SPIE 749 (1987) 37–44.
[10] S.R. Sutton, S. Bajt, J. Delaney, D. Schulze, T. Tokunaga, Rev. Sci. Instr. 66 (2) (1995) 1464–1467.
[11] S. Bajt, S.R. Sutton, J.S. Delaney, Geochim. Cosmochim. Acta 58 (1994) 5209–5214.
[12] S. Bajt, A.L. Hanson, Rev. Sci. Instr. 66 (2, Part II) (1995) 1502–1504.
[13] W.M. Kwiatek, M. Gałka, A.L. Hanson, C. Paluszkiewicz, T. Cichocki, J. Alloys Comp. 328 (2001) 276–282.
[14] O.I. Aruoma, B. Halliwell, E. Gajewski, M. Dizdaroglu, J. Biol. Chem. 264 (1989) 20509–20512.
[15] L.H. Breimer, Mol. Carcinog. 3 (1990) 188–197.
[16] L. Magos, Environ. Health Perspect. 95 (1991) 157–189.